iPLA$_2\beta$: front and center in human monocyte chemotaxis to MCP-1

Ravi S. Mishra,[1] Kevin A. Carnevale,[2] and Martha K. Cathcart[1,3]

[1]Department of Cell Biology, Cleveland Clinic, Cleveland, OH 44195
[2]Department of Pathology, Microbiology and Immunology, University of South Carolina School of Medicine, Columbia, SC 29208
[3]Department of Molecular Medicine, Cleveland Clinic Lerner College of Medicine of Case Western Reserve University, Cleveland, OH 44195

Monocyte chemoattractant protein-1 (MCP-1) directs migration of blood monocytes to inflamed tissues. Despite the central role of chemotaxis in immune responses, the regulation of chemotaxis by signal transduction pathways and their in vivo significance remain to be thoroughly deciphered. In this study, we examined the intracellular location and functions of two recently identified regulators of chemotaxis, Ca^{2+}-independent phospholipase (iPLA$_2\beta$) and cytosolic phospholipase (cPLA$_2\alpha$), and substantiate their in vivo importance. These enzymes are cytoplasmic in unstimulated monocytes. Upon MCP-1 stimulation, iPLA$_2\beta$ is recruited to the membrane-enriched pseudopod. In contrast, cPLA$_2\alpha$ is recruited to the endoplasmic reticulum. Although iPLA$_2\beta$ or cPLA$_2\alpha$ antisense oligodeoxyribonucleotide (ODN)–treated monocytes display reduced speed, iPLA$_2\beta$ also regulates directionality and actin polymerization. iPLA$_2\beta$ or cPLA$_2\alpha$ antisense ODN–treated adoptively transferred mouse monocytes display a profound defect in migration to the peritoneum in vivo. These converging observations reveal that iPLA$_2\beta$ and cPLA$_2\alpha$ regulate monocyte migration from different intracellular locations, with iPLA$_2\beta$ acting as a critical regulator of the cellular compass, and identify them as potential targets for antiinflammatory strategies.

CORRESPONDENCE
Martha K. Cathcart:
cathcam@ccf.org

Abbreviations used: AA, arachidonic acid; AACOCF$_3$, arachidonyl trifluoromethyl ketone; BEL, bromoenol lactone; CCR2, CC chemokine receptor 2; cPLA$_2$, cytosolic phospholipase; DIC, differential interference contrast; iPLA$_2$, Ca^{2+}-independent phospholipase; LPA, lysophosphatidic acid; MCP-1, monocyte chemoattractant protein-1; ODN, oligodeoxyribonucleotide; PA, phosphatidic acid; PDI, protein disulfide isomerase; PI3K, phosphatidylinositol 3-kinase; PLD, phospholipase D; PtdIns(3,4,5)P$_3$, phosphatidylinositol (3,4,5) triphosphate; TBS, Tricine-buffered saline.

Chemokine-induced recruitment of peripheral blood leukocytes to tissues is a critical step in development of inflammatory responses. Hence, specific inhibition of leukocyte migration is envisaged as a rational therapeutic approach for inflammatory diseases (1). Monocyte chemoattractant protein-1 (MCP-1), which is a critical ligand for monocyte chemotaxis, binds to its receptor CC chemokine receptor 2 (CCR2) and recruits monocytes to inflamed sites in a variety of chronic inflammatory diseases, such as atherosclerosis, multiple sclerosis, rheumatoid arthritis, and Alzheimer's disease (2). MCP-1 or CCR2 knockout mice exhibited a severe reduction in monocyte chemotaxis to thioglycolate-induced peritonitis and resistance to atherosclerosis (3–8), suggesting that MCP-1 and CCR2 are required for monocyte migration in both health and disease.

Despite the significance of MCP-1 and monocytes in the pathogenesis of inflammatory diseases, our understanding of how MCP-1 transforms random migration of monocytes to directed migration is limited to identification of a few regulatory signaling molecules. These include phospholipase C (9), Src, Syk, MAPKs p42/44ERK1/2, p38, JNK (10), Pyk2 (unpublished data), phosphatidylinositol 3-kinase (PI3K) (11), protein kinase Cβ (12), and association of Arp2/3 with Wiskott-Aldrich syndrome protein (13). Earlier, we discovered Ca^{2+}-independent phospholipase (iPLA$_2\beta$) and cytosolic phospholipase (cPLA$_2\alpha$) as critical regulators of monocyte chemotaxis to MCP-1. Monocytes rendered deficient in iPLA$_2\beta$ by treatment with antisense oligodeoxyribonucleotides (ODNs) displayed normal cPLA$_2\alpha$ activity, and vice versa. Furthermore, monocytes rendered deficient in iPLA$_2\beta$ or cPLA$_2\alpha$ by their antisense ODNs are restored for chemotaxis to MCP-1 if treated with lysophosphatidic acid (LPA) or arachidonic acid (AA), respectively, yet both enzymes are required for monocyte chemotaxis to MCP-1 (14). These observations led us to hypothesize that iPLA$_2\beta$ and cPLA$_2\alpha$ might be recruited to different intracellular locations, and that they might regulate distinct properties of monocyte chemotaxis to MCP-1. In this study, we tested

The online version of this article contains supplemental material.

these possibilities by examining MCP-1–induced redistribution of these phospholipases and by evaluating their contributions to the characteristics of monocyte chemotaxis to MCP-1. We report that MCP-1 induces iPLA$_2$β recruitment to the membrane-enriched pseudopod, whereas cPLA$_2$α is recruited to the endoplasmic reticulum. Although both enzymes regulate speed and net migration of monocytes toward MCP-1, directionality is governed by iPLA$_2$β, likely by regulating F-actin polymerization. Finally, we validate the requirement for both of these phospholipases for monocyte chemotaxis in vivo using a novel mouse model.

RESULTS

iPLA$_2$β regulates monocyte chemotaxis to MCP-1

The antisense oligodeoxyribonucleotides (AS-ODN) used in our previous study to identify the involvement of iPLA$_2$ was directed against the form of iPLA$_2$ that was eventually classified as iPLA$_2$β (14). iPLA$_2$ isoforms (β/γ) display different sensitivities to R or S enantiomers of the pharmacological inhibitor bromoenol lactone (BEL), with iPLA$_2$β being 10 times more sensitive to (S)-BEL than to (R)-BEL (15). As predicted, (S)-BEL caused stronger reduction of MCP-1–induced monocyte chemotaxis compared with (R)-BEL at all concentrations tested, providing additional evidence that monocyte chemotaxis to MCP-1 is indeed regulated by iPLA$_2$β (Fig. 1 A).

iPLA$_2$β and cPLA$_2$α are recruited to different intracellular sites in response to MCP-1

iPLA$_2$β is recruited to the plasma membrane and the pseudopod. Unstimulated monocytes showed different morphologies that varied from spherical to polar with diffuse, cytoplasmic iPLA$_2$β staining (Fig. 1, C, E, and G, left). Upon MCP-1 stimulation, migrating cells displayed polar morphology, and iPLA$_2$β showed increased distribution at the cell periphery, particularly in the membrane-enriched pseudopod (Fig. 1, C, E, G, right). Quantification of mean fluorescent intensity of iPLA$_2$β in the tail, midbody, and pseudopod of migrating monocytes suggests that, in the absence of MCP-1, iPLA$_2$β was localized predominantly in the tail of monocytes; however, in response to MCP-1, the distribution was reversed and the majority of iPLA$_2$β was detected in the pseudopod of moving cells (Fig. 1 B). These observations demonstrate that MCP-1 induces preferential recruitment of iPLA$_2$β from the tail to the pseudopod of migrating monocytes.

Because MCP-1–induced chemotaxis of iPLA$_2$β-deficient cells could be rescued with LPA (14), which is known to induce focal adhesion assembly (16), it is likely that iPLA$_2$β affects monocyte migration by interacting with an essential component of the pseudopod. Therefore, we evaluated the colocalization of iPLA$_2$β with F-actin and Cdc42, which are two known markers of the pseudopod (Fig. 1, C and E). In the presence of MCP-1, F-actin was enriched in the pseudopod of migrating monocytes and showed increased colocalization with iPLA$_2$β (Fig. 1 C, right, merged image). Quantitative evaluation showed that the MCP-1–induced increased colocalization of F-actin with iPLA$_2$β was not dependent on the polar morphology of monocytes (Fig. 1 D, filled versus black-hatched bar), and that it correlated with significantly enhanced colocalization of iPLA$_2$β with Cdc42 (Fig. 1 E and 1F). Together, these results show that MCP-1 induces redistribution of iPLA$_2$β in nonpolar monocytes that eventually culminates in the increased presence of iPLA$_2$β in the pseudopod of polar monocytes.

Association of iPLA$_2$β with the cell membrane was evaluated by visualizing the colocalization of iPLA$_2$β with Na-K-ATPase (Fig. 1 G). Quantitative evaluation suggested that MCP-1–treated polar monocytes displayed significantly higher colocalization of iPLA$_2$β with Na-K-ATPase compared with untreated monocytes (Fig. 1 H). To rule out the possibility that this was an artifact caused by the small size of the monocytes, the percentage distribution of iPLA$_2$β associated with the cell membrane was also determined by quantifying pixel intensity of iPLA$_2$β on the peripheral cell membrane and in the whole cell (17). As shown in Fig. S1 (available at http://www.jem.org/cgi/content/full/jem.20071243/DC1), MCP-1 induced approximately twofold induction of iPLA$_2$β recruitment to the cell membrane in both polar or nonpolar monocytes, suggesting that recruitment of iPLA$_2$β to the cell membrane is specifically induced by MCP-1, regardless of cell polarity.

cPLA$_2$α is recruited to the endoplasmic reticulum. Because of the stimulus and cell type–dependent variability in intracellular locations of cPLA$_2$α, we initially explored the recruitment of cPLA$_2$α to early endosomes, Golgi, and endoplasmic reticulum by costaining with Rab 5, lectin GS-II, and protein disulfide isomerase (PDI), respectively. cPLA$_2$α showed minimal or no localization with the Golgi or early endosomes (unpublished data). In the absence of MCP-1, cPLA$_2$α was distributed throughout the cytoplasm (Fig. 2 A, left) and did not reveal specific colocalization with PDI (Fig. 2 A, arrowhead). In MCP-1–stimulated cells, cPLA$_2$α was concentrated in the posterior region of the cell and colocalized with PDI (Fig. 2 A, right). MCP-1 induced a significant increase in recruitment of cPLA$_2$α to the endoplasmic reticulum, irrespective of cell polarity (Fig. 2 B, filled versus black-hatched bar).

iPLA$_2$β and cPLA$_2$α do not colocalize. To further substantiate that MCP-1 induces localization of iPLA$_2$β and cPLA$_2$α to different intracellular sites, both enzymes were visualized together, and the percentage of colocalization of the phospholipases was determined. In MCP-1–stimulated monocytes, cPLA$_2$α was concentrated in the posterior main body of the cell; in contrast, iPLA$_2$β was concentrated in the pseudopod (Fig. 2 C, right, merged image). Furthermore, the cPLA$_2$α-rich posterior region was relatively devoid of iPLA$_2$β staining, whereas the iPLA$_2$β-enriched pseudopod showed minimal cPLA$_2$α staining (Fig. 2 C, right, merged image, arrow versus arrowhead). The colocalization of iPLA$_2$β with cPLA$_2$α (28 ± 6%), or vice versa (32 ± 6%), remained statistically unaltered because of MCP-1 treatment (Fig. 2 D).

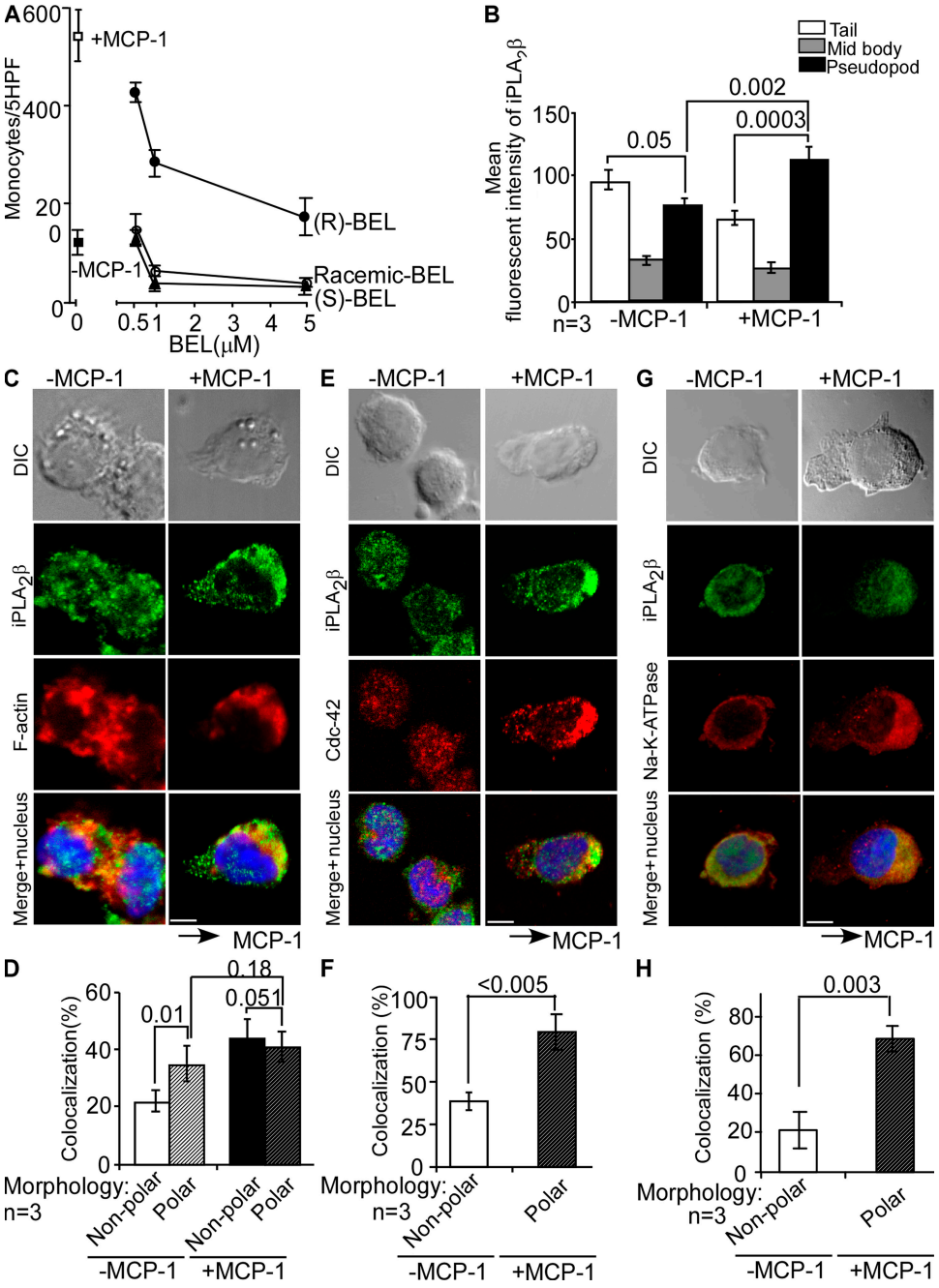

Figure 1. MCP-1 induces recruitment of iPLA$_2$β to the cell membrane–enriched pseudopod of monocytes. (A) To identify the iPLA$_2$ isoform regulating monocyte chemotaxis to MCP-1, monocytes were treated with racemic-BEL (○), (R)-BEL (●), or (S)-BEL (▲) at various concentrations (as indicated) for 1 h at 37°C. Chemotaxis to MCP-1 was assessed using the microchamber assay. Migration of untreated monocytes in the presence (□) and absence (■) of MCP-1 were used as controls. (B) MCP-1 induces redistribution of iPLA$_2$β. The mean fluorescent intensity of iPLA$_2$β in the tail, midbody, and pseudopod of polar monocytes, either in the presence or absence of MCP-1, was determined. Data represent the mean ± the SEM of 40–50 monocytes from 3 independent experiments. (C–H) Colocalization iPLA$_2$β (Alexa Fluor 488) and F-actin, Cdc42, or Na-K ATPase (Alexa Fluor 594) was visualized by observing the distribution of chromophores in a single plane passing through the nucleus. Nuclei were stained with DAPI. Cell morphology was determined by DIC images and statistical analysis was performed using Student's *t* test (two-tailed). Bars, 10 μm. (C) MCP-1–induced translocation of iPLA$_2$β to the pseudopod and localization with F-actin. (D) The effect of MCP-1 on colocalization of iPLA$_2$β with F-actin was quantified in polar and nonpolar monocytes. Data are the mean ± the SEM of 40–50 monocytes. $n = 3$. (E) MCP-1 induced the translocation of iPLA$_2$β to the pseudopod and colocalization with Cdc42. (F) Colocalization (percentage) of iPLA$_2$β with Cdc42 in nonpolar and polar monocytes was quantified. Data represent the mean ± the SEM of 40–50 monocytes. $n = 3$. (G) MCP-1 induced the recruitment of iPLA$_2$β to the cell membrane as visualized with Na-K-ATPase. (H) The quantitative colocalization of iPLA$_2$β with Na-K-ATPase was determined. Monocytes (10–20) from three different experiments were used.

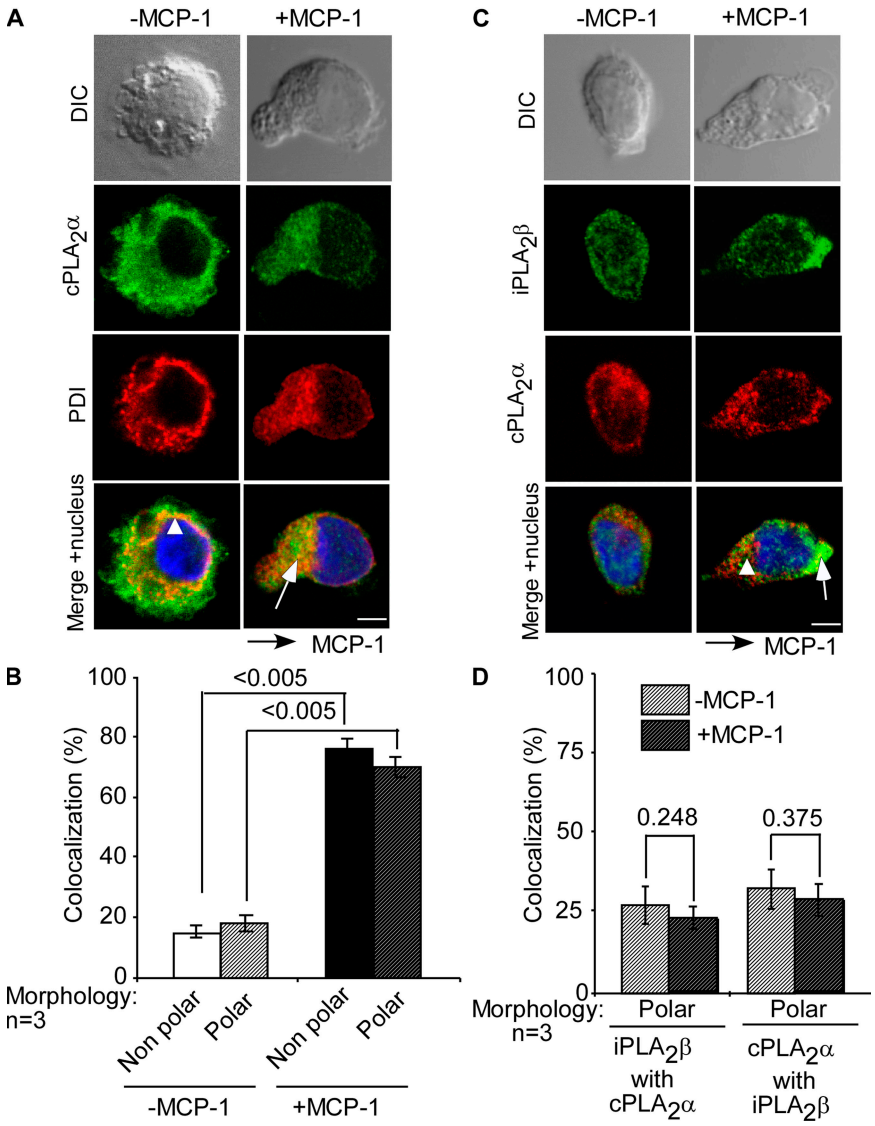

Figure 2. MCP-1 induces translocation of cPLA$_2\alpha$ to the endoplasmic reticulum. (A) cPLA$_2\alpha$ (green) distribution with the endoplasmic reticulum marker PDI (red). Specific colocalization of cPLA$_2\alpha$ with PDI is shown with the white arrow; arrowhead shows an area of no colocalization. (B) Quantitation of colocalization of cPLA$_2\alpha$ with PDI. Data represent the mean ± the SEM of 60 monocytes from three independent experiments. Significance was calculated by an unpaired and two-tailed Student's *t* test. (C) MCP-1–induced differential recruitment of cPLA$_2\alpha$ (red) and iPLA$_2\beta$ (green). (D) Colocalization (percentage) of cPLA$_2\alpha$ with iPLA$_2\beta$, and vice versa, in the same group of monocytes from three independent experiments. Data were plotted as the mean ± the SEM. Statistical significance was determined using an unpaired, two-tailed Student's *t* test. Bars, 10 μm.

In summary, microscopic observations reveal that MCP-1 induces redistribution of both enzymes; cPLA$_2\alpha$ is recruited to the endoplasmic reticulum, whereas iPLA$_2\beta$ is recruited to the membrane-enriched pseudopod of monocytes, and these phospholipases do not colocalize.

iPLA$_2\beta$ and cPLA$_2\alpha$ regulate MCP-1–induced net distance of monocyte migration

To gather insight as to how cPLA$_2\alpha$ and iPLA$_2\beta$ modify chemotaxis of monocytes to MCP-1, we evaluated their effects on the net distance traveled by monocytes in a gradient of MCP-1 using an under-agarose assay. For these studies, we used previously characterized antisense ODNs to assess the effect of iPLA2β and cPLA$_2\alpha$ deficiency on MCP-1–induced chemotaxis of monocytes. It is important to note that these antisense ODNs have been shown to specifically target these enzymes and do not modulate the expression of CCR2 (14, 18, 19). Monocytes were allowed to respond to MCP-1 for 1 h, fixed, and analyzed for net distance. Net distance was determined by measuring the distance of all migrated cells from the periphery of the well to their final position, and it reflects the cumulative effect of change in speed and direction. As shown (Fig. 3), MCP-1 increased the chemotaxis of monocytes and the migrated cells traveled to 1.82-fold greater net distance

(3,082.2 μm) than unstimulated cells (1,722 μm). When treated with iPLA$_2$β antisense ODN, 98.7% reduction was observed in MCP-1–induced chemotaxis (Fig. 3 A). These monocytes displayed reduced net distance (88%) in response to MCP-1 (1,631.4 μm) compared with MCP-1–stimulated cells that were not treated with ODN (Fig. 3 B). Similarly, inhibition of cPLA$_2$α expression with antisense ODN caused 94% reduction in MCP-1–induced chemotaxis (Fig. 3 A) and 84% inhibition of net distance traveled compared with ODN-untreated, MCP-1–unstimulated cells (Fig. 3 B). These observations suggest that, upon MCP-1 stimulation, more monocytes migrate toward MCP-1, and that migrating monocytes travel twice the distance compared with unstimulated cells.

iPLA$_2$β regulates both speed and directionality of monocyte chemotaxis

Reduced net distance of migration of monocytes rendered deficient in phospholipase A$_2$ by antisense ODN, as described in the previous section, in response to MCP-1 (Fig. 3 B) can be caused by a change in the total distance, speed, or net migration of monocytes toward MCP-1 (net-X distance). Therefore, the relative contribution of iPLA$_2$β and cPLA$_2$α to these parameters was delineated by quantitative analysis of time-lapse photomicrographs.

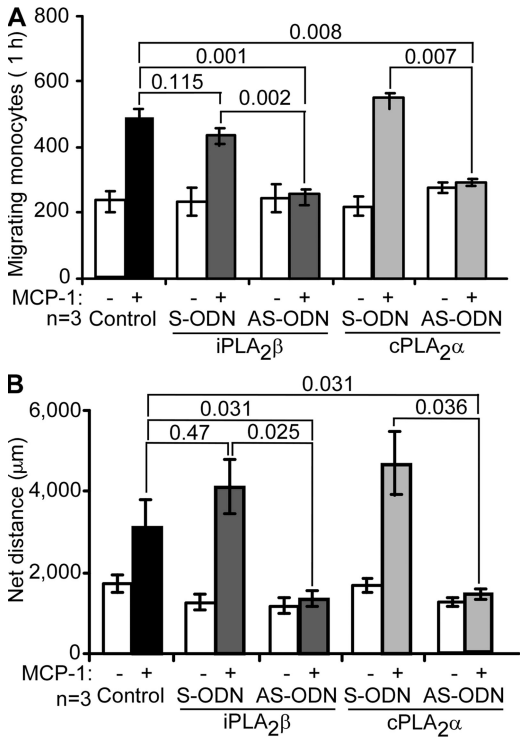

Figure 3. iPLA$_2$β and cPLA$_2$α regulate chemotaxis to MCP-1 in the under-agarose assay. Monocytes treated with antisense ODN of iPLA$_2$β or cPLA$_2$α were migrated for 1 h in response to MCP-1. Composite photomicrographs of the entire field of migration were reconstructed and used for determination of the number of migrating monocytes in the absence or presence of MCP-1 (A) and the net distance traveled by these migrating monocytes (B). The data are expressed as the mean ± the SEM from three independent experiments. Significance was determined by unpaired, one-tailed Student's *t* test.

As shown in wind-rose plots (Fig. 4 A), in the absence of MCP-1, monocytes showed random migration (top left). Upon MCP-1 stimulation, cells migrated toward the source of MCP-1 and traveled longer distances (bottom left). Cells treated with sense ODN to iPLA$_2$β migrated similarly to untreated cells (Fig. 4 A, middle). Interestingly, monocytes treated with iPLA$_2$β antisense ODN showed a more clustered migratory pattern both in the absence or presence of MCP-1 (Fig. 4 A, right top and bottom). Quantitative analysis of all cells that could be tracked for 60 min (*n*) revealed that in response to MCP-1, monocytes migrated significantly faster than unstimulated monocytes and equally to sense ODN–treated cells (Fig. 4 A). In contrast, treatment of monocytes with antisense ODN to iPLA$_2$β significantly decreased the speed of migrating monocytes from 7.58 ± 0.62 to 5.93 ± 0.49 m/min (Fig. 4 A). Furthermore, iPLA$_2$β antisense ODN–treated cells showed a significant reduction in net distance, whereas the net distance traveled by sense ODN-treated monocytes remained unaltered (Fig. 4 C). These findings confirm the results presented in Fig. 3.

We reasoned that speed or net distance merely reflect migration of monocytes, irrespective of their direction. In contrast, the ability of monocytes to reach inflamed sites depends on their ability to navigate toward the source of MCP-1. Hence, the contribution of iPLA$_2$β in directed migration of monocytes toward MCP-1 was determined by quantification of net-X distance that denotes the net value of the X coordinate toward MCP-1. As shown in Fig. 4 D, MCP-1 induced a fivefold induction in net-X. Treatment of monocytes with sense ODN to iPLA$_2$β had no effect; in contrast, monocytes treated with antisense ODN to iPLA$_2$β displayed significant reduction in net-X.

To further probe whether the loss of directionality contributed to the reduced net-X distance (Fig. 4 D) and clustered migratory pattern of iPLA$_2$β antisense ODN-treated monocytes (Fig. 4 A, bottom right), turn analysis was performed. As shown in Fig. 4 E, MCP-1–treated monocytes make fewer wide turns (≥30 degrees, 9 ± 0.81), which is similar to monocytes treated with sense ODN to iPLA$_2$β (9.66 ± 0.76). In contrast, iPLA$_2$β antisense ODN–treated monocytes make more frequent wide turns (>30 degrees, 14.2 ± 1.39). The MCP-1–stimulated monocytes without the ODN treatment showed a significant reduction in average angle per turn from 71.08 ± 7.37 to 35.54 ± 4.18 degrees compared with monocytes without MCP-1 (Fig. 4 F). This effect was totally abrogated in iPLA$_2$β antisense ODN–treated monocytes (Fig. 4 F), suggesting that iPLA$_2$β is a contributor to the cellular compass.

cPLA$_2$α regulates only the speed of monocyte chemotaxis to MCP-1

As shown in Fig. 5 A, wind-rose plots of untreated or monocytes treated with sense ODN to cPLA$_2$α showed random migration in the absence of MCP-1 and directed migration in the presence of MCP-1. Migratory patterns of monocytes treated with

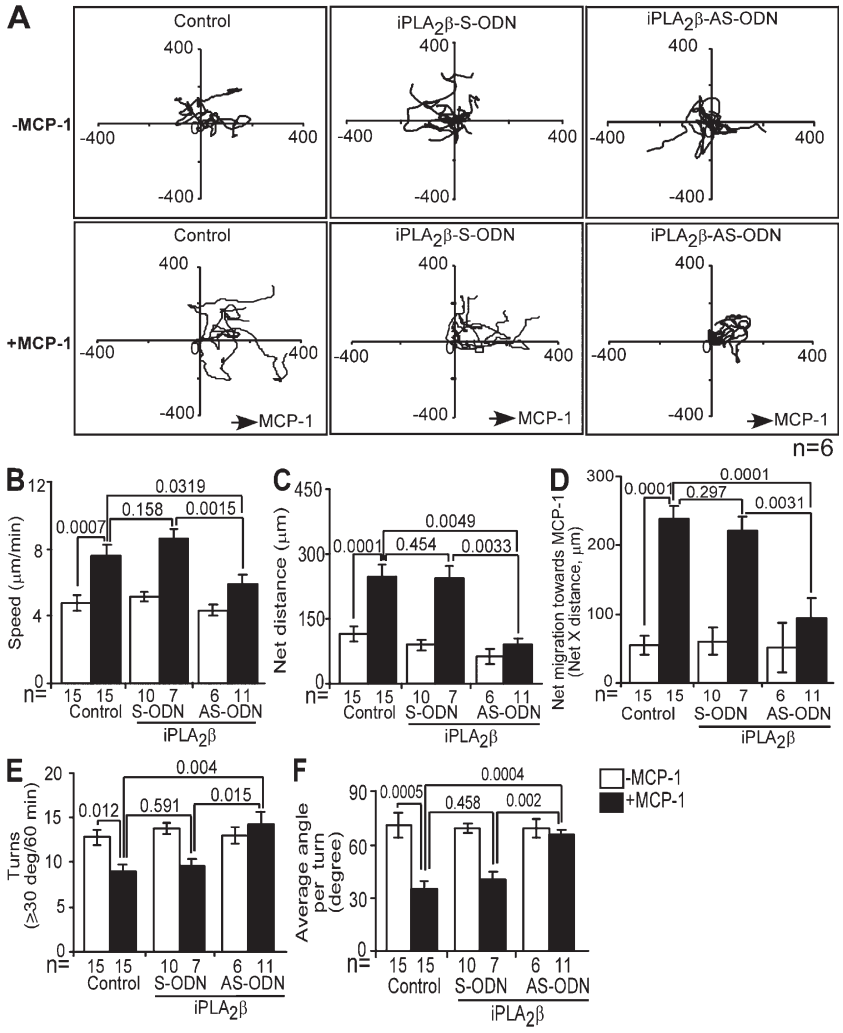

Figure 4. iPLA$_2$β is required for normal speed and directionality of monocytes toward a gradient of MCP-1. Monocytes were tracked at 3-min intervals for 60 min in the presence or absence of MCP-1. (A) Wind-rose plots of monocytes untreated or treated with iPLA$_2$β ODN in the absence or presence of MCP-1. Representative migratory patterns of six monocytes are shown. The effect of iPLA$_2$β antisense ODN treatment on the speed (B), net distance (C), net-X (D), turns ≥30 degrees (E), and average angle/turn (F) of monocytes in the absence or presence of MCP-1. *n*, number of cells analyzed. Data are expressed as the mean ± the SEM. Statistical significance was calculated by Student's *t* test (unpaired, one-tailed [B–D] or unpaired, two-tailed [E and F]).

antisense ODN to cPLA$_2$α were more clustered than the other groups. Quantitative analysis of the migratory patterns of the maximum number of monocytes (*n*) that could be tracked for 60 min revealed that antisense ODN to cPLA$_2$α significantly reduced the speed of monocytes (3.96 ± 0.28 μm/min) compared with ODN-untreated, MCP-1–stimulated cells (7.58 ± 0.62 μm/min; Fig. 5 B). cPLA$_2$α antisense ODN–treated cells also displayed significantly reduced net distance (Fig. 5 C) and net migration toward MCP-1 (net–X distance; Fig. 5 D) compared with either no ODN or sense ODN–treated monocytes. Notably, cPLA$_2$α antisense ODN-treated cells displayed no significant reduction in the number of wide (≥30 degrees) turns or the average angle per turn compared with controls (Fig. 5, E and F). These observations suggest that cPLA$_2$α regulates speed, but not directionality, of monocyte chemotaxis to MCP-1.

iPLA$_2$β regulates F-actin polymerization

MCP-1–induced recruitment of iPLA$_2$β to the F-actin–rich pseudopod and the significant loss of directionality of iPLA$_2$β antisense ODN–treated monocytes suggested that iPLA$_2$β might be involved in actin polymerization. We tested this possibility by evaluating the effect of iPLA$_2$β inhibition on MCP-1–induced actin polymerization. MCP-1 induced a significant increase in the level of F-actin. Interestingly, inhibition of iPLA$_2$β by BEL caused significant reduction in F-actin levels (Fig. 6 A). Furthermore, iPLA$_2$β antisense ODN–treated monocytes displayed a significant reduction in actin polymerization compared with ODN-untreated or iPLA$_2$β sense ODN–treated monocytes (Fig. 6 B). These observations indicate that iPLA$_2$β regulates MCP-1–induced actin polymerization.

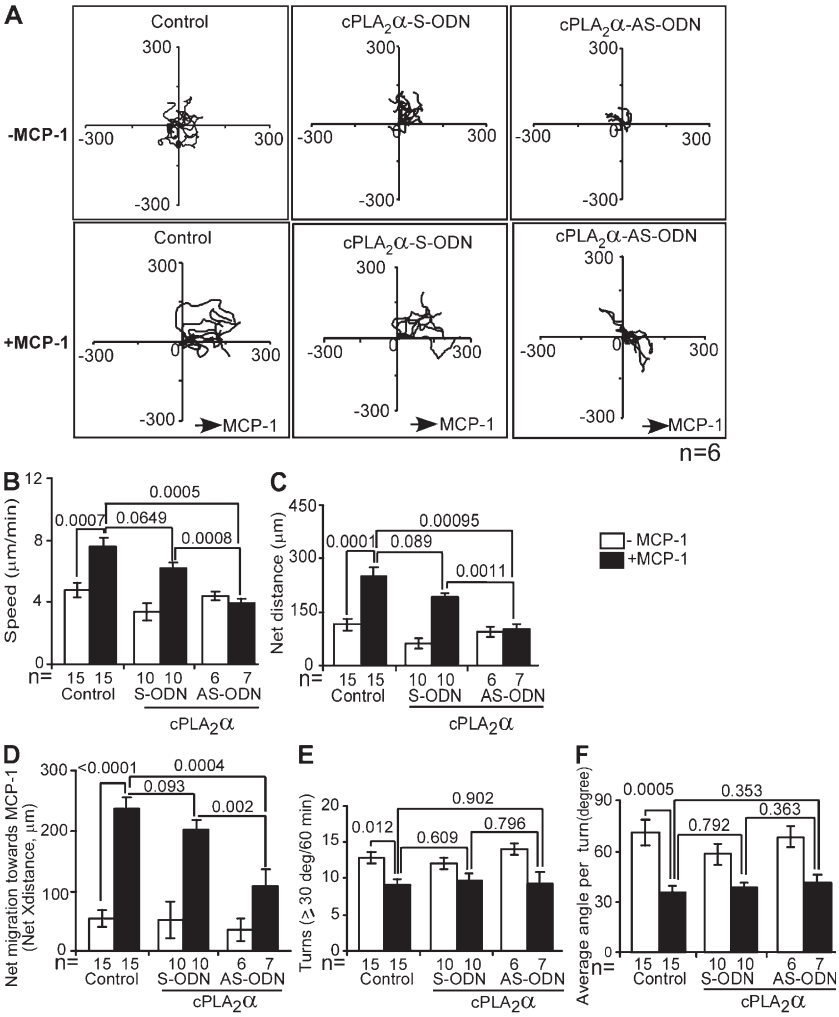

Figure 5. cPLA$_2\alpha$ maintains speed, but not directionality, of monocyte chemotaxis to MCP-1. (A) Wind-rose plots of six representative monocytes untreated or treated with cPLA$_2\alpha$ sense or antisense ODN. The effect of cPLA$_2\alpha$-deficiency on the speed (B), net distance (C), net-X (D), turns ≥30 deg (E), and average angle/turn (F) of monocytes in the presence or absence of MCP-1. *n*, number of the monocytes analyzed. Results shown are the mean ± the SEM. Statistical analysis was performed using Student's *t* test (unpaired, one-tailed [B–D] or unpaired, two-tailed [E and F]).

In vivo validation of the roles of iPLA$_2\beta$ and cPLA$_2\alpha$ in monocyte chemotaxis

We developed a novel adoptive transfer mouse model to validate the regulatory functions of iPLA$_2\beta$ and cPLA$_2\alpha$ in monocyte chemotaxis to MCP-1 in vivo. It is based on the following: (a) migration of monocytes to the peritoneum in thioglycolate-induced peritonitis in wild-type mice is dependent on MCP-1(7); (b) mouse peripheral blood mononuclear cell preparations do not contain neutrophils, and lymphocytes do not respond to MCP-1; (c) monocytes, by virtue of being fluorescently labeled with a stable PKH26, can be distinguished from unlabeled endogenous cells of the recipient mice; (d) we hypothesize that treatment of cells with phospholipase A$_2$–specific inhibitors or antisense ODNs before adoptive transfer will cause migration of fewer adoptively transferred monocytes; and (e) because adoptively transferred cells constitute only a small fraction of total blood cells (11–14%), migration of endogenous leukocytes of the recipient mouse to the peritoneum will not be affected (Fig. 7 A).

Pharmacological inhibition of cPLA$_2\alpha$/iPLA$_2\beta$ suppresses monocyte migration in vivo. Earlier, we reported that the iPLA$_2$ inhibitor racemic-BEL and the cPLA$_2$/iPLA$_2$ inhibitor arachidonyl trifluoromethyl ketone (AACOCF$_3$) both suppressed MCP-1–induced chemotaxis of primary monocytes (14). As predicted from these in vitro data, significantly fewer AACOCF$_3$-treated monocytes migrated to the peritoneum in the adoptive transfer model (Fig. 7 B). Surprisingly, no significant difference was observed in the migration of monocytes treated with racemic-BEL compared with untreated monocytes. The inefficiency of racemic-BEL to inhibit monocyte migration in vivo was found to be caused by time-dependent recovery of BEL-treated monocytes at 37°C in vitro (Fig. S2, available at http://www.jem.org/cgi/content/full/jem.20071243/DC1).

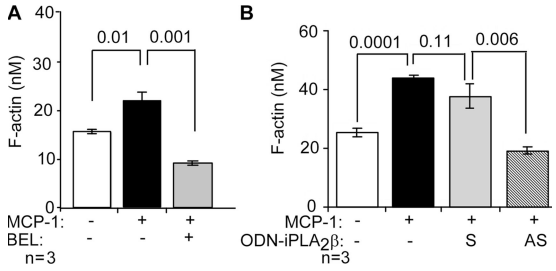

Figure 6. iPLA$_2$β regulates F-actin polymerization in primary human monocytes. (A) Cells were left untreated or treated with racemic-BEL (1 μM for 1 h) and used to determine MCP-1–induced polymerization of actin. (B) Monocytes were left untreated or treated with sense (S-ODN) or antisense ODN (AS-ODN) of iPLA$_2$β. Data are the mean ± the SEM. $n = 3$. Significance was calculated by unpaired, one-tailed Student's t test.

To determine whether the apparent efficacy of AACOCF$_3$ in vivo was caused by toxicity, we examined monocyte survival and chemotaxis to MCP-1 24 h after treatment with AACOCF$_3$ in vitro. As shown in Fig. S3, AACOCF$_3$ treatment did not affect monocyte survival, and the monocytes still displayed significant reduction in chemotaxis to MCP-1 compared with untreated monocytes. These observations suggest that effectiveness of AACOCF$_3$ was caused by the stable inhibitory effect of AACOCF$_3$ on cPLA$_2$α and iPLA$_2$β. As expected, no change was observed in either total monocytes or total leukocytes in the peritoneal lavage (Fig. 7 B).

Phospholipase A$_2$ antisense ODN inhibits MCP-1–mediated chemotaxis of monocytes. Because AACOCF$_3$ inhibits both iPLA$_2$ and cPLA$_2$ and racemic-BEL proved ineffective in vivo, we tested the effect of specific antisense ODNs. iPLA$_2$β antisense ODN used in this study has previously been demonstrated to reduce iPLA$_2$β protein expression in both murine and human monocytes/macrophages (14, 18, 19). It significantly reduced the expression of iPLA$_2$β without affecting cPLA$_2$α protein expression or enzyme activity (14) and was effective in reducing monocyte chemotaxis to MCP-1 in vitro even 24 h later (unpublished data). Similarly, cPLA$_2$α antisense ODN reduced monocyte chemotaxis in vitro without affecting iPLA$_2$β protein expression or enzyme activity (14). It reduced the expression of cPLA$_2$α both in human and murine monocytes (Fig. S4, available at http://www.jem.org/cgi/content/full/jem.20071243/DC1) (14).

As shown (Fig. 8 A), adoptively transferred monocytes treated with iPLA$_2$β antisense ODN displayed statistically significant reduction in migration to the peritoneum compared with untreated or sense ODN–treated monocytes (top). Migration of endogenous monocytes and total leukocytes

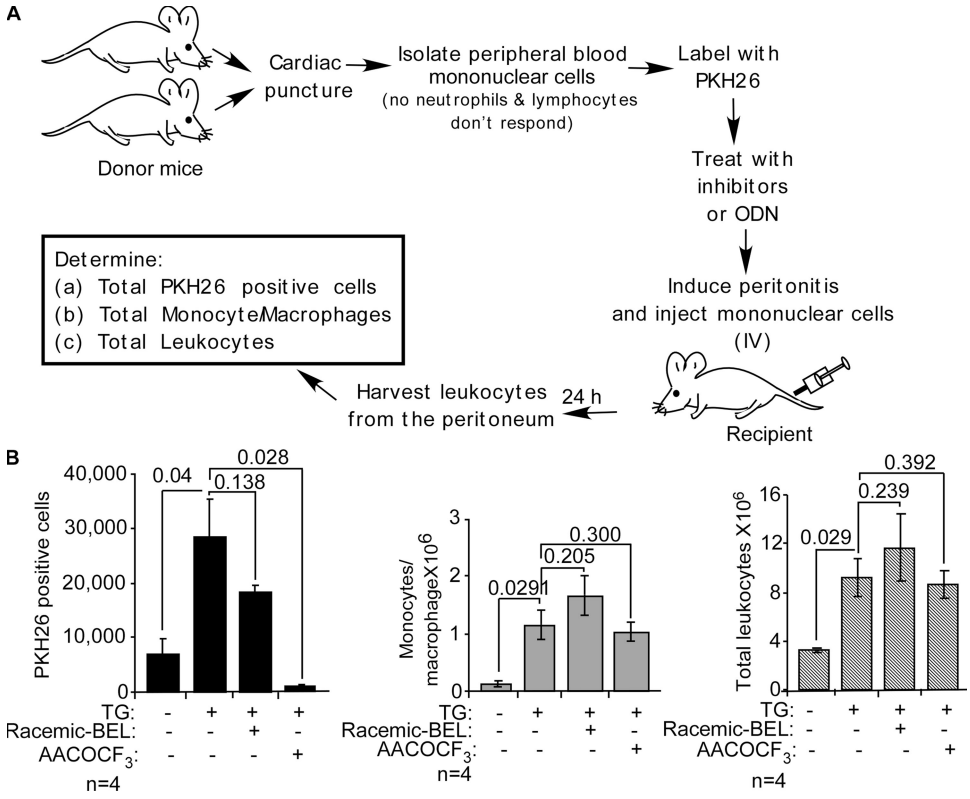

Figure 7. Pharmacological inhibition of PLA$_2$ reduces monocyte chemotaxis to MCP-1 in vivo. (A) Schematic presentation of mouse peritonitis model used as in vivo chemotaxis assay of monocytes to MCP-1. (B) Mouse mononuclear cells left untreated or treated with racemic-BEL (1 μm for 1 h) or AACOCF$_3$ (50 μM for 1 h) were analyzed for migration to peritoneum in response to thioglycolate-induced peritonitis. Cells were scored for adoptively transferred monocytes (left), total monocyte/macrophage (middle), and total leukocytes (right). Data are the mean ± the SEM. $n = 3$.

remained statistically similar. These data suggest that unlike racemic-BEL, iPLA$_2$β antisense ODN–treated monocytes displayed sustained reduced migration in vivo.

To evaluate the in vivo requirement for cPLA$_2$α in MCP-1 chemotaxis, adoptively transferred cells were pretreated with antisense ODN to cPLA$_2$α and monitored for their response to thioglycolate. As shown in Fig. 8 B (top), significantly fewer cPLA$_2$α antisense ODN–treated cells migrated to the peritoneum compared with untreated or cPLA$_2$α sense ODN–treated cells. As expected, infiltration of monocytes (Fig. 8 B, middle) or total leukocytes (Fig. 8 B, bottom) remained unaffected in animals that received either untreated or cPLA$_2$α sense ODN–treated cells. These results demonstrate that iPLA$_2$β and cPLA$_2$α are required for MCP-1–induced chemotaxis of monocytes in vivo, thus validating our previous in vitro findings.

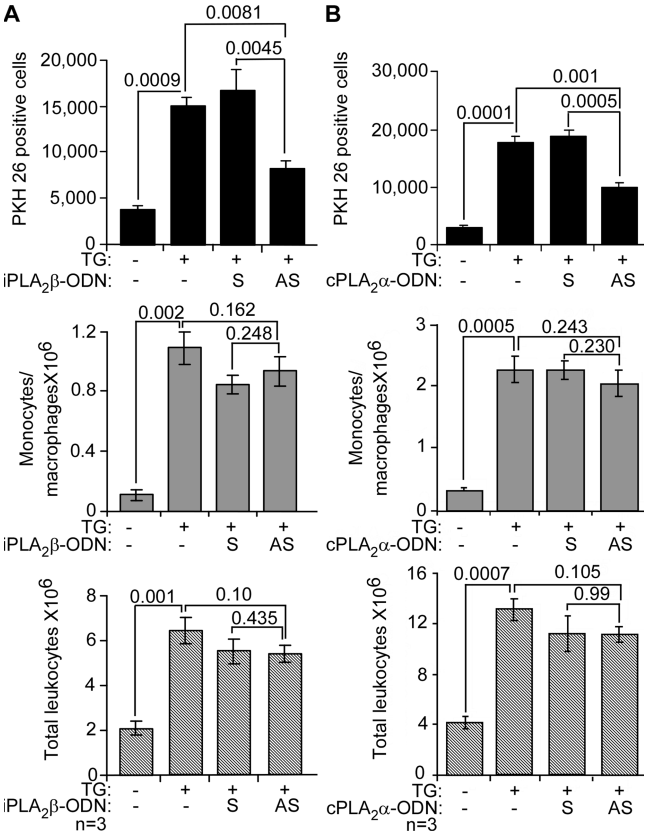

Figure 8. Reduced migration of iPLA$_2$β or cPLA$_2$α AS-ODN–treated mouse monocytes in vivo. (A) Mouse peripheral blood mononuclear cells left untreated or treated with sense (S) or antisense (AS) ODN (5 μm) to iPLA$_2$β (37°C for 24 h) were injected into the recipient mice (1.87 million/recipient). Peritonitis was initiated with thioglycolate. Cells were harvested from the peritoneum after 24 h and scored for PKH26-positive cells (top), monocytes (middle), and total leukocytes (bottom). (B) Mouse mononuclear cells left untreated or treated with cPLA$_2$α sense or antisense ODN were adoptively transferred to recipient mice. Peritonitis was initiated with thioglycolate. After 24 h, peritoneal cells were isolated and scored as indicated in A. Data are the mean ± the SEM. *n* = number of animals.

DISCUSSION

Our studies characterize the important relative contributions of cPLA$_2$α and iPLA$_2$β for regulating monocyte chemotaxis to MCP-1. Reduced migration of adoptively transferred, phospholipase-antisense ODN–treated mouse monocytes to the peritoneum in response to thioglycolate indicates the important signaling roles of iPLA$_2$β and cPLA$_2$α in monocyte chemotaxis to MCP-1 in vivo.

The intracellular locations of these phospholipases vary with the type of cell and nature of stimulus. For example, in INS-1 cells, iPLA$_2$β translocates to the perinuclear region during endoplasmic reticulum stress or stimulation with glucose (20, 21), whereas in smooth muscles cells, iPLA$_2$β is associated with the plasma membrane (22). Similarly, cPLA$_2$α has been reported to be associated with the nuclear membrane, Golgi complex, endoplasmic reticulum, plasma membrane, and an undefined intracellular compartment (23–25). Our observations of the significant increase in colocalization of iPLA$_2$β with membrane and pseudopod markers and of cPLA$_2$α with the ER marker in nonpolar but MCP-1–stimulated monocytes suggest that their recruitment to distinct intracellular locations is induced by MCP-1. This conclusion is further supported by the insignificant colocalization of iPLA$_2$β with cPLA$_2$α, and vice versa.

Earlier, we showed the restoration of chemotaxis of iPLA$_2$β-deficient monocytes to MCP-1 with LPA (14). LPA has been reported to induce phospholipase D (PLD) activity, cytoskeleton rearrangements, and assembly of focal adhesions (26). PLD can generate phosphatidic acid (PA) from membrane phospholipids (27). Interestingly, PA is a preferred substrate of iPLA$_2$β, yielding LPA (28).We have observed that PLD activity is induced by MCP-1 and required for monocyte chemotaxis (unpublished data). Furthermore, PLD is required for LPA-induced cytoskeletal rearrangements, likely through LPA formation (27). As schematically represented in Fig. 9, these observations tempt us to speculate that in response to MCP-1, PLD acts on membrane phospholipids to generate PA, and then iPLA$_2$β acts on PA to liberate LPA. LPA possibly interacts with components of pseudopod assembly and regulates cytoskeletal reorganization; hence, speed and directionality of monocytes. This conjecture is reinforced by observations that actin polymerization is spatially localized to the membrane-enriched pseudopod, where iPLA$_2$β is recruited in response to MCP-1 (Fig. 1, B and C), MCP-1 induces association of iPLA$_2$β with F-actin, irrespective of cell polarity (Fig. 1 D), and MCP-1–induced actin polymerization is significantly reduced in response to iPLA$_2$β inhibition or reduced expression (Fig. 6).

MCP-1 chemotaxis can be restored in cPLA$_2$α-deficient monocytes by AA (14). Thus, cPLA$_2$α may contribute to monocyte migration by generating AA in the endoplasmic reticulum (Fig. 9). AA can be converted into various metabolites, such as prostaglandins, lipoxins, LTB4, and H(P)ETEs via COX-2, cytochrome P450, or lipoxygenase pathways (29). Lipoxins induce RhoA- and Rac-mediated actin reorganization in monocytes/macrophages (30), whereas prostaglandin 2 increases migration of dendritic cells (31). Our observations, in view of

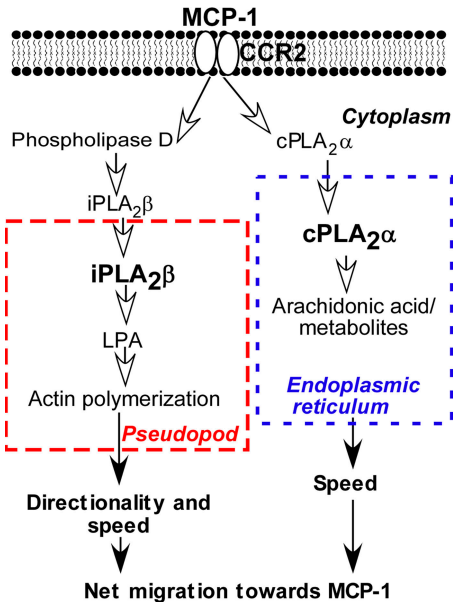

Figure 9. Schematic presentation of the roles of phospholipases A_2 and their lipid products in monocyte chemotaxis to MCP-1. Recognition of MCP-1 by CCR2 activates parallel signaling pathway mediated by $iPLA_2\beta$ and $cPLA_2\alpha$. $iPLA_2\beta$ translocates to the pseudopod and regulates directionality and speed, likely by regulating actin polymerization and thereby inhibiting monocyte chemotaxis. $cPLA_2\alpha$ translocates to the endoplasmic reticulum and regulates monocyte speed through AA or its metabolites. Both enzymes regulate the net migration of monocytes; therefore, deficiency of either of them inhibits chemotaxis of monocytes.

these reports, call for identification of key metabolites of AA that regulate monocyte migration to MCP-1.

Directed cell migration is initiated by sensing of chemotactic stimuli, and culminates in the directed migration of cells. During this process, an external shallow gradient of chemokine is perceived, translated, and amplified into a stable intracellular gradient of signaling molecules that results in the formation of pseudopod at the front and uropod in the rear of a migrating cell. The pseudopod is formed by the activation of the heterotrimeric GTP binding protein Gi, whereas the uropod is formed by the activation of heterotrimeric GTP-binding protein $G_{12/13}$. Phosphatidylinositol (3,4,5) triphosphate (PtdIns[3,4,5]P_3), a key lipid messenger, is synthesized in the leading edge by PI(3)Ks and is degraded by PTEN in the rear edge of migrating cells (32). This vectorial metabolism gives rise to an intracellular gradient of PtdIns(3,4,5)P_3. Pseudopod is organized by Rac/PtdIns(3,4,5)P_3/actin and is stabilized by the scaffold Hem-1 (33, 34). In contrast, the uropod is organized by Rho-mediated, myosin-based contractions (35). This distinct intracellular hierarchy is thought to commence polarity and ensure directed migration of cells in a chemokine gradient. Multiple signaling molecules are believed to orchestrate these distinct events at the opposing edges of a migrating cell. For example, Cdc42 regulates stability and location of the leading edge, whereas Rac, which transforms random migration of fibroblasts and epithelial cells to directed migration (36), only controls morphological and invasion characteristics of macrophages (37). Vav1 is supposed to control the speed of migrating macrophages (38). In neutrophils, deficiency of Rho GEF Lsc causes faster migration and loss of directionality (39), whereas deficiency of PI3Kγ causes only loss of directionality (40). In *Dictyostelium discoideum,* PTEN regulates levels of PtdIns(3,4,5)P_3; in contrast, in neutrophils, it is metabolized by the PtdIns(3,4,5)P_3 phosphatase SHIP1 rather than PTEN. These observations not only point toward evolution of cell-based variability in key signaling molecules, they also provide an impetus to search for unknown members of these cascades (41, 42).

Once considered a probable cellular compass, recent reports suggest that PtdIns(3,4,5)P_3 is primarily a component of positive-feedback loop controlling persistent actin dynamics (43). Emerging concepts argue for the existence of parallel signaling pathways for chemotaxis and indicate that an unknown cellular compass exists upstream of PI3Kγ (42, 44). Interestingly, a calcium-independent phospholipase (PLA_2A) that liberates AA from phosphatidylcholine and acts in parallel with PI3K/PTEN has recently been implicated in chemotaxis of *D. discoideum* (45). Because $iPLA_2$ does not show a preference for the fatty acyl moiety at the sn-2 position of phospholipids, and *D. discoideum* does not contain $cPLA_2\alpha$, it is possible that PLA_2A merely performs twin functions of $cPLA_2\alpha$ and $iPLA_2\beta$ by liberating LPA and AA. Our observations on loss of directionality of $iPLA_2\beta$-deficient monocytes raise the possibility that $iPLA_2\beta$ is either a cellular compass or a component of a cellular compass. Our observations, together with recent reports (44, 45), suggest that phospholipases are critical components of parallel signaling pathways regulating monocyte chemotaxis as schematically represented in Fig. 9. How $iPLA_2\beta$ directs monocytes toward MCP-1, as well as whether it is a universal regulator of chemotaxis, remains to be deciphered. One key function ascribed to $iPLA_2\beta$ is membrane remodeling and membrane trafficking that brings about changes in shape and fluidity of the plasma membrane (46). It will be interesting to explore whether $iPLA_2\beta$ regulates monocyte chemotaxis by changing lipid composition of membrane rafts, thereby modifying assembly of signaling molecules in the pseudopod of migrating cells (47).

The impaired in vivo migration of adoptively transferred mouse monocytes that contain either inactive PLA_2 (by $AACOCF_3$) or were rendered deficient in PLA_2 by AS-ODN validates our in vitro observations (14) in a dynamic in vivo milieu. We now have adapted this in vivo assay to monitor human monocyte chemotaxis (48). Our reports show the importance of in vitro studies for identification of potential signaling components. Our in vivo MCP-1 chemotaxis assay provides a straightforward approach to verify the relevance of signaling pathways that appear promising for regulating MCP-1–dependent chemotaxis in vitro.

In summary, our studies provide insight into how two seemingly similar phospholipases regulate directed migration of monocytes from different intracellular sites. We report that MCP-1 induces chemotaxis of monocytes by increasing speed, as well as introducing directionality. By translocating to the

pseudopod and regulating directionality and speed, iPLA$_2\beta$ acts front and center, whereas in contrast, cPLA$_2\alpha$ is recruited to the endoplasmic reticulum and regulates only speed. The profound defects in migration of iPLA$_2\beta$- or cPLA$_2\alpha$-deficient mouse monocytes in vivo validate the important roles for these enzymes in regulating extravasation of blood monocytes to sites of inflammation.

MATERIALS AND METHODS

Antibodies and reagents

BEL and AACOCF$_3$ were obtained from Biomol. Bel enantiomers (R and S) were provided by R. Gross (Washington University School of Medicine, St. Louis, MO). Human recombinant MCP-1 (BD Biosciences) was used at a concentration of 5.75 nM. Anti-iPLA$_2\beta$ (1:50; goat polyclonal), anti–human Cdc-42 (1:50; rabbit polyclonal), and anti–human PDI (1:100; rabbit polyclonal) were purchased from Santa Cruz Biotechnology. Anti–human cPLA$_2\alpha$ (rabbit polyclonal) and a mouse monoclonal antibody against human Na-K ATPase (1:200) were obtained from Cell Signaling Technology. Rhodamine phalloidin (1:40), Rab5, lectin GSII-Alexa Fluor 594, and Alexa Fluor 594– or 488–tagged species-specific secondary antibody raised in donkey (1:200) were obtained from Invitrogen.

Isolation of human monocytes and cell culture

Human monocytes were isolated from freshly drawn human whole blood, as described by McNally et al. (49), and maintained in DME (10% BCS) in polypropylene tubes at 2×10^6 cells/ml. Studies on human monocytes were approved by the Institutional Review Board of the Cleveland Clinic.

Chemotaxis assays

Microchamber chemotaxis assay. This assay was performed as previously described (14) and was used to quantify monocyte migration to MCP-1.

Under-agarose cell migration assay. The under-agarose cell migration assay was performed as described by Heit and Kubes (50) using 10% BCS containing DME. Net distance in this assay denotes the distance between the edge of the well and the final position of migrating cells. It was determined from the composite photomicrograph of the entire field of migration.

Treatment of monocytes with pharmacological inhibitors and antisense ODNs

Monocytes were pretreated with Racemic-BEL or its R or S enantiomers (0.1–5 μM) or AACOCF$_3$ (50 μM) at 37°C in 10% CO_2 for 1 h, and washed in serum-free DME before being used for chemotaxis. The sense and antisense ODN sequences for phospholipases used in this study were phosphorothioate modified and purified by HPLC (Sigma-Aldrich). These ODNs were of proven efficacy and specificity, and were delivered under standardized experimental conditions, as described (14). These specific antisense ODNs were effective in reducing the expression of iPLA$_2\beta$ or cPLA$_2\alpha$, as described in our previous study (14).

Immunostaining and confocal microscopy

Monocytes were allowed to migrate using the under-agarose cell migration assay (1 h), fixed, and permeabilized with Triton X-100 (0.1% in PBS for 4 min). Nonspecific sites were blocked with 3% BSA in PBS (37°C for 1 h). Cells were incubated with primary antibody (for 1 h at 37°C), washed, and visualized with fluorescently labeled secondary antibody (for 1 h at 37°C). Stained cells were mounted in Vectashield (Vector Laboratories) and observed using a laser-scanning confocal microscope (DMR XE attached to TCS SP2; Leica). Horizontal sections were imaged using a 63× objective (magnification 5×, pinhole 1, and format of 1,024 × 1,024). Images were analyzed by Image-Pro Plus (Media Cybernetics) and processed using Photoshop CS (Adobe).

Time-lapse microscopy

For this purpose, under-agarose cell migration was performed in serum-coated polystyrene six-well culture dishes, essentially as described in the previous section. The plate was placed on a preheated stage at 37°C under 10% CO_2. Images were acquired with an inverted microscope (DMIRB; Leica) using a 10× phase objective. Images were acquired at 3-min intervals using 30-ms exposure times and recorded with a cooled charge-coupled device camera (Cool SNAP HQ; Roper Scientific) using Metamorph software (Universal Image).

Image analysis

Image analysis was conducted with Image-Pro Plus. In the absence of MCP-1, randomly migrating cells often return to the well where they originated. Because of the large number of cells in the well itself, returning cells could not be followed after reentering the well. Therefore, cells that can be tracked for the 60-min duration were used for migration analysis. Total distance depicts total length of a migratory path, speed denotes total distance/60 min, and net distance depicts the linear distance between the first and the last position of a migrating cell. Net-X is the net value of the X coordinate after 60 min. The turn angle is the absolute value of the angle between successive positions of migrating cell measured from the direction of the preceding position. Average angle/turn depicts the average angles of the turns taken by a migrating cell during 60 min of migration at 3-min intervals.

Quantification and colocalization of phospholipases

Mean fluorescent intensity of iPLA$_2\beta$ in tail, midbody, and pseudopod of polar cells was determined by measuring pixel intensity of iPLA$_2\beta$ and area clearly demarcated based on cellular morphology shown by differential interference contrast (DIC) images using Image-Pro Plus. Colocalization (percentage) of enzymes with marker proteins were determined as previously described (51).

Determination of F-actin

This assay was used to determine the effect of iPLA$_2\beta$ inhibition on F-actin polymerization, as described by Finkel et al. (52) using 2 million cells.

Isolation of mouse peripheral blood mononuclear cells

Animals (BALB/CJ; Jackson ImmunoResearch Laboratory) were used according to the protocol approved by the Cleveland Clinic Foundation Institutional Animal Care and Use Committee. BALB/CJ female mice (7–8 mo, two donors per recipient) were anesthetized with avertin (0.4 ml/animal). Blood was collected by cardiac puncture in a 1-ml syringe containing 0.05 ml of EDTA (0.5 M). Blood (10 ml) was diluted with 10 ml of Tricine-buffered saline (TBS; 10 mM, pH 7.4) and mixed with 5 ml of OptiPrep (Sigma-Aldrich). Blood was transferred to a suitable tube, overlayed with 0.5 ml of TBS and centrifuged at 1,000 *g* for 30 min at 20°C without the brake. The supernatant, containing mononuclear cells, was collected, diluted with 2 volumes of TBS, and centrifuged at 400 *g* for 10 min. The pellet was reconstituted in 0.5 ml of TBS, layered on dialyzed calf serum (2 ml), and centrifuged at 200 *g* for 15 min to remove platelets. Cells were suspended in TBS and counted. The recovery of mononuclear cells by this method was 7.45×10^4/g mouse.

Fluorescent labeling of mononuclear cells with PKH26

Cells were labeled per the manufacturer's instructions. Cells were suspended in DMEM and treated with inhibitors as previously described (14).

Adoptive transfer of mononuclear cells and initiation of peritonitis

Recipient mice (3–4 per group) were lightly anesthetized with avertin. Peritoneal inflammation was induced by thioglycolate injection (1 ml, 4% in physiological saline) into the peritoneal cavity. Tail veins were dilated with limonene and cleaned with 95% ethanol. The labeled mononuclear cells (1.4–1.8 million per animal) were injected into the tail vein, and the time of injection was recorded. Injected cells represent only 11–14% of total peripheral blood mononuclear cells of similar weight recipient animals. After 24 h, peritoneal cells were harvested, washed, resuspended in PBS (1 ml), and counted. Cells were fixed and used to prepare 10 cytospins for each sample. Half of them were

stained with HEMA per the manufacturer's (Thermo Fisher Scientific) instruction, to determine the number of monocytes. The remainder was mounted in Vectashield. PKH26-positive cells were counted on an upright microscope (model DMR; Leica) using a Texas red filter.

Statistical analysis

Statistical significance of observations was calculated using the Student's *t* tests. $P < 0.05$ was considered significant.

Online supplemental material

Fig. S1 presents data indicating that MCP-1 induces membrane localization of $iPLA_2\beta$ in both polar and nonpolar monocytes. Fig. S2 demonstrates the transient nature of BEL inhibition of monocyte chemotaxis to MCP-1 in a time-dependent manner. Fig. S3 shows the stable inhibitory effect of $AACOCF_3$ on monocyte chemotaxis to MCP-1, and that $AACOCF_3$ does not affect monocyte viability under these conditions. Fig. S4 shows inhibition of $cPLA_2\alpha$ protein expression in murine monocytes/macrophages by treatment with antisense ODN. Supplemental materials and methods are also provided. The online version of this article is available at http://www.jem.org/cgi/content/full/jem.20071243/DC1.

The authors thank Dr. Richard Gross for the gift of BEL enantiomers; Amit Vasanji for help with image analysis; and Drs. Josephine Adams and Ashish Bhattacharjee for their helpful comments.

This study is supported by National Institutes of Health grants (HL 510681 and HL 61971) to M.K. Cathcart and by the General Clinical Research Center Grant M01-RR-018390.

The authors have no competing financial interests.

Submitted: 19 June 2007
Accepted: 21 December 2007

REFERENCES

1. Luster, A.D., R. Alon, and U.H. von Andrian. 2005. Immune cell migration in inflammation: present and future therapeutic targets. *Nat. Immunol.* 6:1182–1190.
2. Dawson, J., W. Miltz, A.K. Mir, and C. Wiessner. 2003. Targeting monocyte chemoattractant protein-1 signalling in disease. *Expert Opin. Ther. Targets.* 7:35–48.
3. Wyss-Coray, T., J.D. Loike, T.C. Brionne, E. Lu, R. Anankov, F. Yan, S.C. Silverstein, and J. Husemann. 2003. Adult mouse astrocytes degrade amyloid-beta in vitro and in situ. *Nat. Med.* 9:453–457.
4. Kurihara, T., G. Warr, J. Loy, and R. Bravo. 1997. Defects in macrophage recruitment and host defense in mice lacking the CCR2 chemokine receptor. *J. Exp. Med.* 186:1757–1762.
5. Gu, L., Y. Okada, S.K. Clinton, C. Gerard, G.K. Sukhova, P. Libby, and B.J. Rollins. 1998. Absence of monocyte chemoattractant protein-1 reduces atherosclerosis in low density lipoprotein receptor-deficient mice. *Mol. Cell.* 2:275–281.
6. Kuziel, W.A., S.J. Morgan, T.C. Dawson, S. Griffin, O. Smithies, K. Ley, and N. Maeda. 1997. Severe reduction in leukocyte adhesion and monocyte extravasation in mice deficient in CC chemokine receptor 2. *Proc. Natl. Acad. Sci. USA.* 94:12053–12058.
7. Lu, B., B.J. Rutledge, L. Gu, J. Fiorillo, N.W. Lukacs, S.L. Kunkel, R. North, C. Gerard, and B.J. Rollins. 1998. Abnormalities in monocyte recruitment and cytokine expression in monocyte chemoattractant protein 1–deficient mice. *J. Exp. Med.* 187:601–608.
8. Boring, L., J. Gosling, M. Cleary, and I.F. Charo. 1998. Decreased lesion formation in CCR2−/− mice reveals a role for chemokines in the initiation of atherosclerosis. *Nature.* 394:894–897.
9. Kuang, Y., Y. Wu, H. Jiang, and D. Wu. 1996. Selective G protein coupling by C-C chemokine receptors. *J. Biol. Chem.* 271:3975–3978.
10. Cambien, B., M. Pomeranz, M.A. Millet, B. Rossi, and A. Schmid-Alliana. 2001. Signal transduction involved in MCP-1-mediated monocytic transendothelial migration. *Blood.* 97:359–366.
11. Jones, G.E., E. Prigmore, R. Calvez, C. Hogan, G.A. Dunn, E. Hirsch, M.P. Wymann, and A.J. Ridley. 2003. Requirement for PI 3-kinase gamma in macrophage migration to MCP-1 and CSF-1. *Exp. Cell Res.* 290:120–131.
12. Carnevale, K.A., and M.K. Cathcart. 2003. Protein kinase C beta is required for human monocyte chemotaxis to MCP-1. *J. Biol. Chem.* 278:25317–25322.
13. Mukai, Y., K. Iwaya, H. Ogawa, and K. Mukai. 2005. Involvement of Arp2/3 complex in MCP-1-induced chemotaxis. *Biochem. Biophys. Res. Commun.* 334:395–402.
14. Carnevale, K.A., and M.K. Cathcart. 2001. Calcium-independent phospholipase A(2) is required for human monocyte chemotaxis to monocyte chemoattractant protein 1. *J. Immunol.* 167:3414–3421.
15. Moran, J.M., R.M. Buller, J. McHowat, J. Turk, M. Wohltmann, R.W. Gross, and J.A. Corbett. 2005. Genetic and pharmacologic evidence that calcium-independent phospholipase A2beta regulates virus-induced inducible nitric-oxide synthase expression by macrophages. *J. Biol. Chem.* 280:28162–28168.
16. Ridley, A.J., and A. Hall. 1992. The small GTP-binding protein rho regulates the assembly of focal adhesions and actin stress fibers in response to growth factors. *Cell.* 70:389–399.
17. Wustner, D., M. Mondal, I. Tabas, and F.R. Maxfield. 2005. Direct observation of rapid internalization and intracellular transport of sterol by macrophage foam cells. *Traffic.* 6:396–412.
18. Balsinde, J., M.A. Balboa, and E.A. Dennis. 1997. Antisense inhibition of group VI Ca2+-independent phospholipase A2 blocks phospholipid fatty acid remodeling in murine P388D1 macrophages. *J. Biol. Chem.* 272:29317–29321.
19. Balboa, M.A., and J. Balsinde. 2002. Involvement of calcium-independent phospholipase A2 in hydrogen peroxide-induced accumulation of free fatty acids in human U937 cells. *J. Biol. Chem.* 277:40384–40389.
20. Ramanadham, S., F.F. Hsu, S. Zhang, C. Jin, A. Bohrer, H. Song, S. Bao, Z. Ma, and J. Turk. 2004. Apoptosis of insulin-secreting cells induced by endoplasmic reticulum stress is amplified by overexpression of group VIA calcium-independent phospholipase A2 (iPLA2 beta) and suppressed by inhibition of iPLA2 beta. *Biochemistry.* 43:918–930.
21. Bao, S., C. Jin, S. Zhang, J. Turk, Z. Ma, and S. Ramanadham. 2004. Beta-cell calcium-independent group VIA phospholipase A(2) (iPLA(2)beta): tracking iPLA(2)beta movements in response to stimulation with insulin secretagogues in INS-1 cells. *Diabetes.* 53:S186–S189.
22. Bolotina, V.M. 2004. Store-operated channels: diversity and activation mechanisms. *Sci. STKE.* 2004:pe34.
23. Sierra-Honigmann, M.R., J.R. Bradley, and J.S. Pober. 1996. "Cytosolic" phospholipase A2 is in the nucleus of subconfluent endothelial cells but confined to the cytoplasm of confluent endothelial cells and redistributes to the nuclear envelope and cell junctions upon histamine stimulation. *Lab. Invest.* 74:684–695.
24. Kan, H., Y. Ruan, and K.U. Malik. 1996. Involvement of mitogen-activated protein kinase and translocation of cytosolic phospholipase A2 to the nuclear envelope in acetylcholine-induced prostacyclin synthesis in rabbit coronary endothelial cells. *Mol. Pharmacol.* 50:1139–1147.
25. Herbert, S.P., S. Ponnambalam, and J.H. Walker. 2005. Cytosolic phospholipase A2-alpha mediates endothelial cell proliferation and is inactivated by association with the Golgi apparatus. *Mol. Biol. Cell.* 16:3800–3809.
26. Tou, J.S., and J.S. Gill. 2005. Lysophosphatidic acid increases phosphatidic acid formation, phospholipase D activity and degranulation by human neutrophils. *Cell. Signal.* 17:77–82.
27. Kam, Y., and J.H. Exton. 2001. Phospholipase D activity is required for actin stress fiber formation in fibroblasts. *Mol. Cell. Biol.* 21:4055–4066.
28. Tang, J., R.W. Kriz, N. Wolfman, M. Shaffer, J. Seehra, and S.S. Jones. 1997. A novel cytosolic calcium-independent phospholipase A2 contains eight ankyrin motifs. *J. Biol. Chem.* 272:8567–8575.
29. Osterud, B., and E. Bjorklid. 2003. Role of monocytes in atherogenesis. *Physiol. Rev.* 83:1069–1112.
30. Maderna, P., D.C. Cottell, G. Berlasconi, N.A. Petasis, H.R. Brady, and C. Godson. 2002. Lipoxins induce actin reorganization in monocytes and macrophages but not in neutrophils: differential involvement of rho GTPases. *Am. J. Pathol.* 160:2275–2283.
31. van Helden, S.F., D.J. Krooshoop, K.C. Broers, R.A. Raymakers, C.G. Figdor, and F.N. van Leeuwen. 2006. A critical role for prostaglandin E2

in podosome dissolution and induction of high-speed migration during dendritic cell maturation. *J. Immunol.* 177:1567–1574.
32. Ridley, A.J., M.A. Schwartz, K. Burridge, R.A. Firtel, M.H. Ginsberg, G. Borisy, J.T. Parsons, and A.R. Horwitz. 2003. Cell migration: integrating signals from front to back. *Science.* 302:1704–1709.
33. Srinivasan, S., F. Wang, S. Glavas, A. Ott, F. Hofmann, K. Aktories, D. Kalman, and H.R. Bourne. 2003. Rac and Cdc42 play distinct roles in regulating PI(3,4,5)P3 and polarity during neutrophil chemotaxis. *J. Cell Biol.* 160:375–385.
34. Weiner, O.D., M.C. Rentel, A. Ott, G.E. Brown, M. Jedrychowski, M.B. Yaffe, S.P. Gygi, L.C. Cantley, H.R. Bourne, and M.W. Kirschner. 2006. Hem-1 complexes are essential for Rac activation, actin polymerization, and myosin regulation during neutrophil chemotaxis. *PLoS Biol.* 4:e38.
35. Kimura, K., M. Ito, M. Amano, K. Chihara, Y. Fukata, M. Nakafuku, B. Yamamori, J. Feng, T. Nakano, K. Okawa, et al. 1996. Regulation of myosin phosphatase by Rho and Rho-associated kinase (Rho-kinase). *Science.* 273:245–248.
36. Pankov, R., Y. Endo, S. Even-Ram, M. Araki, K. Clark, E. Cukierman, K. Matsumoto, and K.M. Yamada. 2005. A Rac switch regulates random versus directionally persistent cell migration. *J. Cell Biol.* 170:793–802.
37. Wheeler, A.P., C.M. Wells, S.D. Smith, F.M. Vega, R.B. Henderson, V.L. Tybulewicz, and A.J. Ridley. 2006. Rac1 and Rac2 regulate macrophage morphology but are not essential for migration. *J. Cell Sci.* 119:2749–2757.
38. Wells, C.M., P.J. Bhavsar, I.R. Evans, E. Vigorito, M. Turner, V. Tybulewicz, and A.J. Ridley. 2005. Vav1 and Vav2 play different roles in macrophage migration and cytoskeletal organization. *Exp. Cell Res.* 310:303–310.
39. Francis, S.A., X. Shen, J.B. Young, P. Kaul, and D.J. Lerner. 2006. Rho GEF Lsc is required for normal polarization, migration, and adhesion of formyl-peptide-stimulated neutrophils. *Blood.* 107:1627–1635.
40. Hannigan, M., L. Zhan, Z. Li, Y. Ai, D. Wu, and C.K. Huang. 2002. Neutrophils lacking phosphoinositide 3-kinase gamma show loss of directionality during N-formyl-Met-Leu-Phe-induced chemotaxis. *Proc. Natl. Acad. Sci. USA.* 99:3603–3608.
41. Nishio, M., K. Watanabe, J. Sasaki, C. Taya, S. Takasuga, R. Iizuka, T. Balla, M. Yamazaki, H. Watanabe, R. Itoh, et al. 2007. Control of cell polarity and motility by the PtdIns(3,4,5)P3 phosphatase SHIP1. *Nat. Cell Biol.* 9:36–44.
42. Franca-Koh, J., Y. Kamimura, and P.N. Devreotes. 2007. Leading-edge research: PtdIns(3,4,5)P3 and directed migration. *Nat. Cell Biol.* 9:15–17.
43. Ferguson, G.J., L. Milne, S. Kulkarni, T. Sasaki, S. Walker, S. Andrews, T. Crabbe, P. Finan, G. Jones, S. Jackson, et al. 2007. PI(3)Kgamma has an important context-dependent role in neutrophil chemokinesis. *Nat. Cell Biol.* 9:86–91.
44. Van Haastert, P.J., and D.M. Veltman. 2007. Chemotaxis: navigating by multiple signaling pathways. *Sci. STKE.* 2007:pe40.
45. Chen, L., M. Iijima, M. Tang, M.A. Landree, Y.E. Huang, Y. Xiong, P.A. Iglesias, and P.N. Devreotes. 2007. PLA2 and PI3K/PTEN pathways act in parallel to mediate chemotaxis. *Dev. Cell.* 12:603–614.
46. Brown, W.J., K. Chambers, and A. Doody. 2003. Phospholipase A2 (PLA2) enzymes in membrane trafficking: mediators of membrane shape and function. *Traffic.* 4:214–221.
47. Gomez-Mouton, C., R.A. Lacalle, E. Mira, S. Jimenez-Baranda, D.F. Barber, A.C. Carrera, A.C. Martinez, and S. Manes. 2004. Dynamic redistribution of raft domains as an organizing platform for signaling during cell chemotaxis. *J. Cell Biol.* 164:759–768.
48. Bhattacharjee, A., R.S. Mishra, G. Feldman, and M.K. Cathcart. 2008. In vivo validation of signaling pathways regulating human monocyte chemotaxis. *J. Immunol. Methods.* In press.
49. McNally, A.K., G.M. Chisolm III, D.W. Morel, and M.K. Cathcart. 1990. Activated human monocytes oxidize low-density lipoprotein by a lipoxygenase-dependent pathway. *J. Immunol.* 145:254–259.
50. Heit, B., and P. Kubes. 2003. Measuring chemotaxis and chemokinesis: the under-agarose cell migration assay. *Sci. STKE.* 2003:PL5.
51. Low, S.H., A. Vasanji, J. Nanduri, M. He, N. Sharma, M. Koo, J. Drazba, and T. Weimbs. 2006. Syntaxins 3 and 4 are concentrated in separate clusters on the plasma membrane before the establishment of cell polarity. *Mol. Biol. Cell.* 17:977–989.
52. Finkel, T., J.A. Theriot, K.R. Dise, G.F. Tomaselli, and P.J. Goldschmidt-Clermont. 1994. Dynamic actin structures stabilized by profilin. *Proc. Natl. Acad. Sci. USA.* 91:1510–1514.